

Absence of $4a_0$ superlattice in bulk kagome superconductor CsV_3Sb_5

Haoxiang Li,¹ Yu-Xiao Jiang,² J. X. Yin,² Sangmoon Yoon,¹ Andrew R. Lupini,³ C. Nelson,⁴ A. H. Said,⁵ Y. M. Yang,⁶ H. C. Lei,⁷ Binghai Yan,⁸ Ziqiang Wang,⁹ M. Z. Hasan,² H. N. Lee,¹ and H. Miao^{1,*}

¹*Material Science and Technology Division, Oak Ridge National Laboratory, Oak Ridge, Tennessee 37831, USA*

²*Laboratory for Topological Quantum Matter and Advanced Spectroscopy (B7),*

Department of Physics, Princeton, New Jersey 08544, USA

³*Center for Nanophase Materials Sciences, Oak Ridge National Laboratory, Oak Ridge, TN, USA*

⁴*National Synchrotron Light Source II, Brookhaven National Laboratory, Upton, NY 11973, USA*

⁵*Advanced Photon Source, Argonne National Laboratory, Argonne, Illinois 60439, USA*

⁶*School of information science and engineering, Shandong University, Qingdao, 266237, China*

⁷*Department of Physics and Beijing Key Laboratory of Opto-Electronic Functional Materials and Micro-devices, Renmin University of China, Beijing, China*

⁸*Department of Condensed Matter Physics, Weizmann Institute of Science, Rehovot 7610001, Israel*

⁹*Department of Physics, Boston College, Chestnut Hill, Massachusetts 02467, USA*

(Dated: November 24, 2021)

The kagome superconductor AV_3Sb_5 ($\text{A}=\text{K}, \text{Rb}, \text{Cs}$) is a rare platform to explore the interplay between topology, geometrical frustration and symmetry-breaking orders. In addition to the charge density wave below $T_{CDW} \sim 94$ K and superconductivity below $T_{SC} \sim 3$ K, recent surface sensitive studies of CsV_3Sb_5 find evidence of 1×4 superlattices below $T^* \sim 60$ K. Interestingly, this unidirectional $4a_0$ phase may intertwine with charge density wave and superconductivity and possibly responsible for spectroscopic and transport anomalies below T^* . Here, combining high-resolution X-ray diffraction and scanning tunneling microscopy, we demonstrate that the 1×4 superstructure emerges uniquely on the surface and hence exclude the $4a_0$ phase as the origin of T^* anomaly in the bulk CsV_3Sb_5 .

Kagome lattice is a geometrically frustrated structure that features flat band, Dirac fermion and van Hove singularity in its electronic structure. Near the van Hove filling, the high density of state together with the orthogonal wave-functions on sub-lattices are predicted to support unconventional symmetry breaking orders such as the p -wave charge/spin density waves, d -wave Pomeranchuk instability and f -wave superconductivity [1–6].

Recently, a topological kagome metal AV_3Sb_5 ($\text{A}=\text{K}, \text{Rb}, \text{Cs}$), possessing a vanadium kagome layer (Fig. 1a-b), is discovered to host unconventional and intertwined electronic orders. Figure 1c-e depict the temperature dependent symmetry-breaking of CsV_3Sb_5 . At room temperature, CsV_3Sb_5 has an ideal kagome structure that has D_{6h} space group and preserves the time-reversal symmetry, \mathcal{T} . Below $T_{CDW} \sim 94$ K, a three-dimensional charge density wave [7–12] accompanies with an inverse star-of-David lattice distortion emerges [13, 14] and breaks translational and C_6 -rotational symmetries [6, 13, 14]. Near the same temperature, evidence of \mathcal{T} -breaking has been observed [9, 11, 15–19], supporting a CDW with imaginary hopping terms [4–6]. At $T_{SC} \sim 3$ K, CsV_3Sb_5 enters to a superconducting phase that breaks the $U(1)$ gauge symmetry. Interestingly, at an intermediate temperature, $T^* \sim 60$ K, an additional unidirectional $4a_0$ charge modulation is observed by scanning tunneling spectroscopy studies [20–22].

As shown in Fig. 1e, the $4a_0$ phase is transparent to thermodynamic measurement, however, anomaly

lies below T^* has been observed in Raman scattering [7, 23], ultrafast pump-probe reflectivity [12, 22], muon spin relaxation [18], transport [24] and nuclear magnetic/quadrupole resonance (NMR/NQR) [25] measurements, pointing connections between the $4a_0$ phase and T^* anomaly. In addition, while the three-dimensional $2 \times 2 \times 2$ CDW has been identified below T_{CDW} [7, 8, 11, 14], more recent hard x-ray diffraction found evidence of $2 \times 2 \times 4$ superstructure at low temperature [10], adding another layer of complexity on the interplay between electronic symmetry breaking and lattice distortions. Here we combine meV-resolution hard x-ray diffraction (meV-XRD), scanning tunneling microscopy (STM) to demonstrate that the $4a_0$ phase exist only on the surface of CsV_3Sb_5 and exclude its relevance to the T^* anomaly in CsV_3Sb_5 .

We first establish the surface modulations of CsV_3Sb_5 with STM at 4.2 K. Figure 1f shows the topographic image of clean Sb surfaces. In agreement with previous STM studies [20–22], the Fourier transformation of the topography, shown in Fig. 1g, reveals both 2×2 and 1×4 superlattice modulations. Figure 1h and i show The dI/dV images at ± 20 meV, respectively. As highlighted between the black lines, the maximum charge intensity of the $4a_0$ phase at 20 meV turns to the lowest charge intensity at -20 meV, demonstrating a charge intensity reversal and consistent with Peierls-type CDW [26–28].

To search for the 1×4 superstructure peak in the bulk crystal of CsV_3Sb_5 , we perform meV-XRD study in transmission geometry as shown in Fig. 2a. The bandwidth of incident energy is 1 meV; this is done using a high-resolution monochromator (HRM) that consists of

* miaoh@ornl.gov

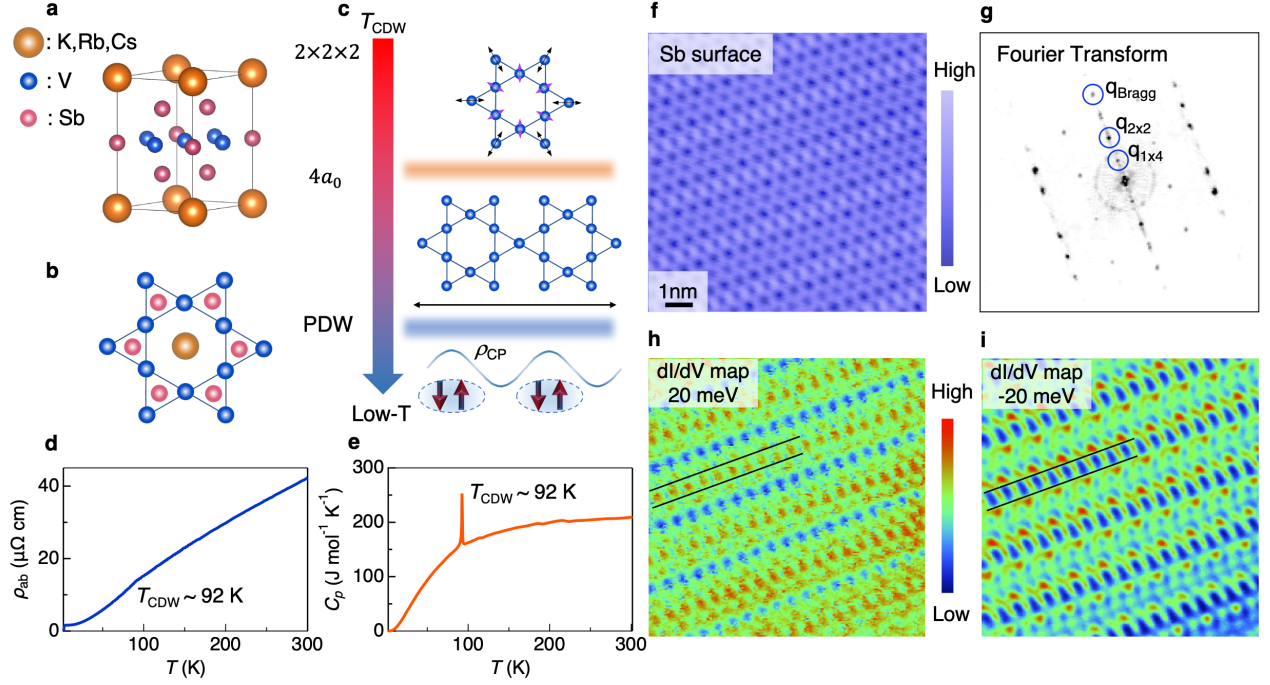


Figure 1. The crystal structure of AV_3Sb_5 and temperature dependent symmetry breaking phases of CsV_3Sb_5 . **a.** the crystal structure of AV_3Sb_5 (space group $P6/mmm$, No. 191). It consists of V-Sb slabs that are separated by alkali elements. **b.** The V-Sb slab contains a V-kagome lattice and two Sb sites laying in the kagome plane and above the V-triangle. **c.** Schematic of temperature-dependent symmetry-breaking phases in CsV_3Sb_5 . Panel **d**, **e** shows resistivity and specific heat of CsV_3Sb_5 , respectively. **(f)** Topographic image of a clean Sb surface ($V = -100$ mV, $I = 0.5$ nA). **(g)** Fourier transform of the topography showing Bragg peaks and charge ordering vector peaks. The in-plane 2×2 CDW, 1×4 charge order and Bragg peaks are highlighted by circles. **(h)** and **(i)** show atomically resolved dI/dV imaging for the same Sb surface at energy $E = -20$ meV and $E = +20$ meV, respectively. The inset shows the underlying $4a_0$ charge order inferred from the simultaneously obtained topographic image.

six silicon crystals [29, 30]. The meV-beam is then focused to lateral size of $15 \times 35 \mu m^2$ (vertical \times horizontal). A total $\Delta E = 1.5$ meV energy resolution is achieved by matching the incident photon energy, $h\nu = 23.72$ keV, to the backscattering energy of Si(12,12,12). The extremely high energy resolution filters out background intensity [31] and false peaks appearing in conventional XRD (see supplementary fig. S1 [32]). Figure 2b shows the scattering trajectories along the high symmetry directions, *i.e.*, $[1,0,0]$ (H -scan), $[0,1,0]$ (K -scan), $[1,-1,0]$ and $[1,1,0]$ (HK -scan) in reciprocal lattice unit (r.l.u.). Figure 2c-h present base temperature ($T = 10$ K) H , K and HK -scans at the $L = 0$ and $L = 2$ plane. Peaks at $H = 0.5$ and/or $K = 0.5$ are corresponding to the CDW superlattice peak. Through all scattering trajectories, we do not observe 1×4 superstructure peaks locate at $q = 0.25$ or 0.75 r.l.u. This observation is in stark contrast with STM result shown in Fig. 1g, where the $4a_0$ superstructure peak intensity is comparable with the in-plane 2×2 CDW peak. These results thus demonstrate that the $4a_0$ phase in CsV_3Sb_5 is a surface/interface effect.

The surface origin of the $4a_0$ phase is indeed consistent with recent density functional theory study, where the 1×4 superstructure is stabilized by the relative shift be-

tween V-atoms and surface Sb-atoms [19, 35]. However, the absence of $4a_0$ phase in bulk CsV_3Sb_5 raises question on the origin of T^* anomalies in other bulk sensitive measurements [7, 12, 18, 22, 24, 25]. Recent NMR/NQR study [25] suggested that the T^* anomaly could be related to the $2 \times 2 \times 4$ superstructure observed in previous XRD study [10]. To further explore this possibility, we perform the XRD measurement with reflection geometry to search for superstructure peaks along the out-of-plane direction. Interestingly, as shown in Fig. 3, while we confirm the $L = 0.25$ superlattice peaks, these peaks persist up to room temperature in our high precision measurement. In contrast, the CDW peak at $L = 0.5$ disappears above T_{CDW} , consistent with transport and specific heat measurement shown in Fig. 1(d) and (e). We, therefore, conclude that the $2 \times 2 \times 4$ superstructure is also irrelevant to the T^* anomaly and likely a consequence of $4c_0$ stacking fault in this material (c_0 is the out-of-plane lattice constant). Indeed, XRD measurement along other Q paths (Fig. 3b,c) present more superstructure peaks with $3c_0$ ($L \sim 0.33$) and $7c_0$ ($L \sim 0.14$ r.l.u.) lattice modulations. Surprisingly, we found that the correlation length, defined as inverse half-width-at-half-maximum ($1/HWHM$) [7, 33, 34], of $L = 0.14, 0.25$,

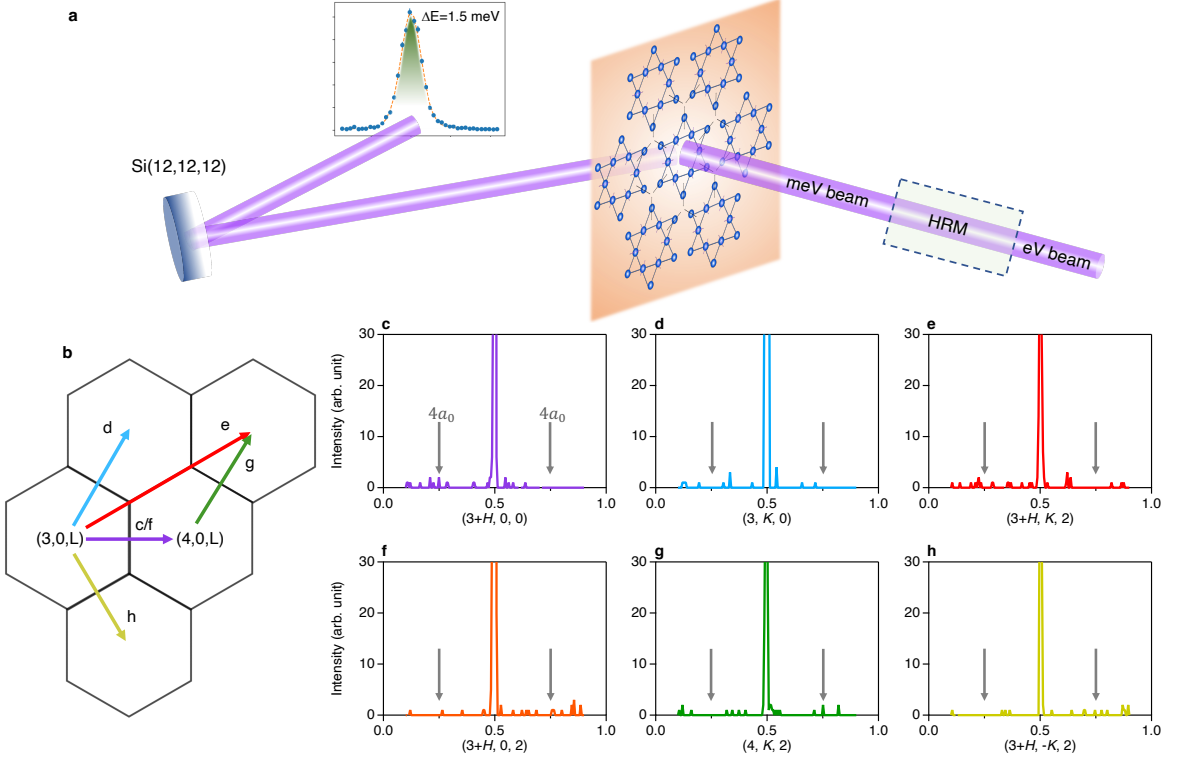


Figure 2. Absence of $4a_0$ superlattice peak in meV-XRD measurement. **a** Schematics of the experimental setup for the meV-XRD measurement. The inset spectrum reveals the total energy resolution of ~ 1.5 meV (FWHM). **b** Schematics indicating the scattering trajectories for meV-XRD scans shown in panel **c** to **h**. Measurements were performed at 10 K and covered all in-plane high symmetry directions with zero and finite L components. The $2 \times 2 \times 2$ CDW peaks can be clearly resolved in all scans, but there is no peak feature at $q = 0.25$ or 0.75 (highlighted by the grey arrows), demonstrating the absence of the $4a_0$ superlattice in bulk CsV_3Sb_5 .

0.33, 0.5 superlattice peaks are 115, 257, 61, 480 Å, suggesting mesoscopic structural phase separation.

Our high precision XRD study excludes translational symmetry breaking as the origin of T^* anomalies. It is worth noting that while the in-plane 2×2 charge modulation preserves C_6 symmetry, the 3-dimensional $2 \times 2 \times 2$ superstructure breaks the rotational symmetry down to C_2 [13]. This twofold rotation symmetry breaking is induced by the π phase shift between the adjacent kagome layers that reduces the crystal symmetry from D_{6h} to D_{2h} [6, 13]. We therefore conclude that neither translational symmetry nor rotational symmetry breaking drives the T^* anomaly. Recently, evidence of time-reversal symmetry breaking is observed in both KV_3Sb_5 and CsV_3Sb_5 [9, 11, 15–18], it will be interesting to evaluate the interplay between time-reversal symmetry and spatial symmetry and their relevance to the T^* anomaly.

In summary, combining high-precision XRD and STM, we demonstrate that the $2 \times 2 \times 2$ CDW is the only spatial symmetry breaking below the room temperature. Our results highlight the novel surface/interface effects of CsV_3Sb_5 and shed light on the origin of T^* anomaly in CsV_3Sb_5 .

I. METHOD

A. Sample preparation and characterizations

Single crystals of CsV_3Sb_5 were grown from Cs ingot (purity 99.9%), V powder (purity 99.9%) and Sb grains (purity 99.999%) using the self-flux method, similar to the growth of RbV_3Sb_5 [36]. The mixture was put into an alumina crucible and sealed in a quartz ampoule under partial argon atmosphere. The sealed quartz ampoule was heated to 1273 K for 12 h and soaked there for 24 h. Then it was cooled down to 1173 K at 50 K/h and further to 923 K at a slowly rate. Finally, the ampoule was taken out from the furnace and decanted with a centrifuge to separate CsV_3Sb_5 single crystals from the flux. The obtained crystals have a typical size of $2 \times 2 \times 0.02$ mm³. CDW transitions are clearly observed in transport and specific heat measurement shown in Fig. 1d and e, respectively.

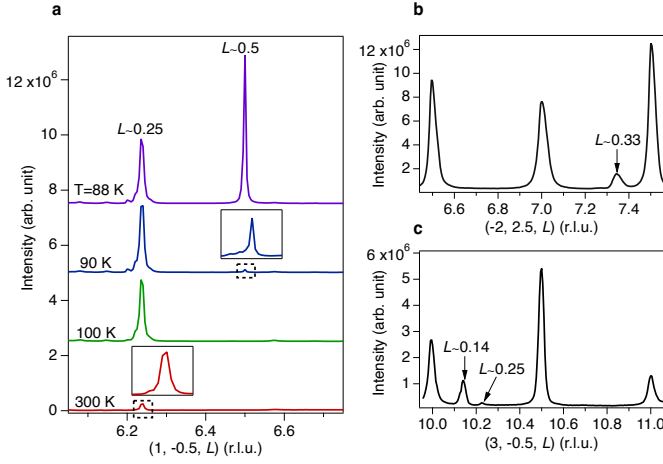


Figure 3. Out-of-plane superstructure peaks. **a.** Temperature dependent XRD measurement from $\mathbf{Q}=(1, -0.5, 6.05)$ to $(1, -0.5, 6.75)$. The CDW peak at $L=6.5$ disappear above the $T_{CDW} \sim 94$ K, whereas the superstructure peak at $L=6.25$ persist up to room temperature. **b-c.** Two out-of-plane scan taken at $T=70$ K that show superstructure peak at $L=0.33$ and $L=0.14$, which correspond to $3c_0$ and $7c_0$ superlattices. By fitting the superstructure peaks with a Lorentzian-squared function [33, 34], we extract HWHM of each peak, which is 0.013, 0.006, 0.024, 0.003 r.l.u. for $L=0.14, 0.25, 0.33, 0.5$ r.l.u., respectively. The correlation length, defined as inverse HWHM ($1/\text{HWHM}$), is 115, 257, 61, 480 Å for $L=0.14, 0.25, 0.33, 0.5$ r.l.u., respectively.

B. Hard X-ray diffraction

High-precision X-ray scattering measurements were performed at 30-ID-C (HERIX) of Advanced Photon Source (APS) and 4-ID beamline of NSLS-II. Data shown in Fig. 2 was taken at 30-ID-C (HERIX), where the highly monochromatic x-ray beam of incident energy $E_i = 23.7$ keV ($\lambda = 0.5226$ Å) was focused on the sample with a beam cross section of $35 \times 15 \mu\text{m}^2$ (horizontal \times vertical). The total energy resolution of the monochromatic x-ray beam and analyzer crystals was $\Delta E \sim 1.5$ meV (full width at half maximum). The measurements were performed in transmission geometry. Data shown in Fig. 3 was taken at 4-ID beamline of NSLS-II. The photon energy, which was selected by a cryogenically-cooled Si(111) double-crystal monochromator, was 11.47 keV. The sample was mounted in a closed-cycle displx cryostat in a vertical scattering geometry, and the sigma-sigma scattering channel was measured using a MgO(440) polarization analyzer and silicon drift detector.

II. SUPPLEMENTARY INFORMATION

A. Energy resolution effect in XRD

Figure S1 compares the XRD data without (red) and with (purple) MgO(440) analyzer. In the data taken

without the analyzer, a sharp peak appears at $q \sim 0.26$ r.l.u., which intensity is much higher than that of the CDW peak at $q \sim 0.5$ r.l.u. Other broad background signals with comparable intensity to the CDW peak also appears in the data. These extrinsic features fully disappear in the data with the analyzer. It is important to note, multiple weak peaks can be identified in the purple curve, which could be falsely interpreted as superlattice structures at low temperature. These extra peaks are completely gone in our meV-XRD measurement.

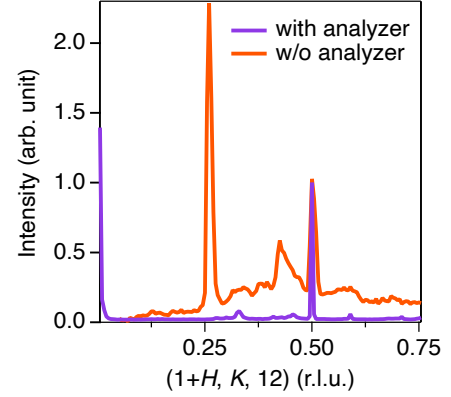


Figure S1. XRD measurement of CsV_3Sb_5 at $T=10$ K, scanning from $\mathbf{Q}=(1,0,12)$ to $(2,1,12)$. To reveal the energy resolution effect, we compare the XRD spectra taken with (purple) and without (orange) a MgO(440) polarization analyzer that greatly reduce the scattered beam bandwidth. The spectrum taken without analyzer shows a sharp peak at $q \sim 0.26$ r.l.u., together with multiple broad background peaks near the CDW peak at $q \sim 0.5$ r.l.u.. The $q \sim 0.26$ peak and the broad background signal can effectively be filtered.

III. ACKNOWLEDGEMENT

We thank Kun Jiang, Jiaqiang Yan and Michael McGuire for stimulating discussions. This research was sponsored by the U.S. Department of Energy, Office of Science, Basic Energy Sciences, Materials Sciences and Engineering Division and by the Laboratory Directed Research and Development Program of Oak Ridge National Laboratory, managed by UT-Battelle, LLC, for the U. S. Department of Energy. H.C.L. was supported by National Natural Science Foundation of China (Grant No. 11822412 and 11774423), Ministry of Science and Technology of China (Grant No. 2018YFE0202600 and 2016YFA0300504) and Beijing Natural Science Foundation (Grant No. Z200005). Z.Q.W. is supported by the U.S. Department of Energy, Basic Energy Sciences Grant No. DE-FG02-99ER45747. B.Y. acknowledges the financial support by the Willner Family Leadership Institute for the Weizmann Institute of Science, the Benozio Endowment Fund for the Advancement of Science, Ruth and Herman Albert Scholars Program for New Scientists,

the European Research Council (ERC) under the European Union's Horizon 2020 research and innovation programme (Grant No. 815869) and ISF MAFAT Quantum Science and Technology (2074/19). This research uses resources (meV-IXS experiment at beam line 30-ID) of the Advanced Photon Source, a U.S. DOE Office of Science User Facility operated for the DOE Office of Science by Argonne National Laboratory under Contract No. DE-AC02-06CH11357. Hard-x-ray diffraction measurements

use resources at the 4-ID beam line of the National Synchrotron Light Source II, a U.S. Department of Energy Office of Science User Facility operated for the DOE Office of Science by Brookhaven National Laboratory under Contract No. DE-SC0012704. Extraordinary facility operations are supported in part by the DOE Office of Science through the National Virtual Biotechnology Laboratory, a consortium of DOE national laboratories focused on the response to COVID-19, with funding provided by the Coronavirus CARES Act.

-
- [1] W.-S. Wang, Z.-Z. Li, Y.-Y. Xiang, and Q.-H. Wang, Competing electronic orders on kagome lattices at van hove filling, *Phys. Rev. B* **87**, 115135 (2013).
 - [2] M. L. Kiesel, C. Platt, and R. Thomale, Unconventional fermi surface instabilities in the kagome hubbard model, *Phys. Rev. Lett.* **110**, 126405 (2013).
 - [3] X. Feng, K. Jiang, Z. Wang, and J. Hu, Chiral flux phase in the kagome superconductor av_3sb_5 , *Science Bulletin* **66**, 1384 (2021).
 - [4] M. M. Denner, R. Thomale, and T. Neupert, Analysis of charge order in the kagome metal av_3sb_5 ($a = \text{k, rb, cs}$) (2021), arXiv:2103.14045 [cond-mat.str-el].
 - [5] Y.-P. Lin and R. M. Nandkishore, Complex charge density waves at van hove singularity on hexagonal lattices: Haldane-model phase diagram and potential realization in kagome metals av_3sb_5 (2021), arXiv:2104.02725 [cond-mat.supr-con].
 - [6] T. Park, M. Ye, and L. Balents, Electronic instabilities of kagome metals: saddle points and landau theory (2021), arXiv:2104.08425 [cond-mat.supr-con].
 - [7] H. X. Li, T. T. Zhang, T. Yilmaz, Y. Y. Pai, C. Marvinney, A. Said, Q. Yin, C. Gong, Z. Tu, E. Vescovo, C. S. Nelson, R. G. Moore, S. Murakami, H. C. Lei, H. N. Lee, B. Lawrie, and H. Miao, Observation of unconventional charge density wave without acoustic phonon anomaly in kagome superconductors av_3sb_5 ($a = \text{rb, cs}$) (2021), arXiv:2103.09769 [cond-mat.supr-con].
 - [8] Z. Liang, X. Hou, F. Zhang, W. Ma, P. Wu, Z. Zhang, F. Yu, J.-J. Ying, K. Jiang, L. Shan, Z. Wang, and X.-H. Chen, Three-dimensional charge density wave and surface-dependent vortex-core states in a kagome superconductor csv_3sb_5 , *Phys. Rev. X* **11**, 031026 (2021).
 - [9] D.W.Song, L.X.Zheng, F.H.Yu, J.Li, L.P.Nie, M.Shan, D.Zhao, S.J.Li, B.L.Kang, Z.M.Wu, Y.B.Zhou, K.L.Sun, K.Liu, X.G.Luo, Z.Y.Wang, J.J.Ying, X.G.Wan, T.Wu, and X. H. Chen, Orbital ordering and fluctuations in a kagome superconductor csv_3sb_5 (2021), arXiv:2104.09173 [cond-mat.supr-con].
 - [10] B. R. Ortiz, S. M. L. Teicher, L. Kautzsch, P. M. Sarte, J. P. C. Ruff, R. Seshadri, and S. D. Wilson, Fermi surface mapping and the nature of charge density wave order in the kagome superconductor csv_3sb_5 (2021), arXiv:2104.07230 [cond-mat.supr-con].
 - [11] F. H. Yu, T. Wu, Z. Y. Wang, B. Lei, W. Z. Zhuo, J. J. Ying, and X. H. Chen, Concurrence of anomalous hall effect and charge density wave in a superconducting topological kagome metal (2021), arXiv:2102.10987 [cond-mat.str-el].
 - [12] N. Ratcliff, L. Hallett, B. R. Ortiz, S. D. Wilson, and J. W. Harter, Coherent phonon spectroscopy and inter-layer modulation of charge density wave order in the kagome metals csv_3sb_5 (2021), arXiv:2104.10138 [cond-mat.supr-con].
 - [13] H. Miao, H. X. Li, H. N. Lee, A. Said, H. C. Lei, J. X. Yin, M. Z. Hasan, Z. Wang, H. Tan, and B. Yan, Geometry of the charge density wave in kagome metal av_3sb_5 (2021), arXiv:2106.10150 [cond-mat.str-el].
 - [14] H. Tan, Y. Liu, Z. Wang, and B. Yan, Charge density waves and electronic properties of superconducting kagome metals (2021), arXiv:2103.06325 [cond-mat.supr-con].
 - [15] S.-Y. Yang, Y. Wang, B. R. Ortiz, D. Liu, J. Gayles, E. Derunova, R. Gonzalez-Hernandez, L. Šmejkal, Y. Chen, S. S. P. Parkin, S. D. Wilson, E. S. Toberer, T. McQueen, and M. N. Ali, Giant, unconventional anomalous Hall effect in the metallic frustrated magnet candidate, KV_3Sb_5 , *Science Advances* **6**, 10.1126/sciadv.abb6003 (2020).
 - [16] Y.-X. Jiang, J.-X. Yin, M. M. Denner, N. Shumiya, B. R. Ortiz, G. Xu, Z. Guguchia, J. He, M. S. Hossain, X. Liu, J. Ruff, L. Kautzsch, S. S. Zhang, G. Chang, I. Belopolski, Q. Zhang, T. A. Cochran, D. Multer, M. Litskevich, Z.-J. Cheng, X. P. Yang, Z. Wang, R. Thomale, T. Neupert, S. D. Wilson, and M. Z. Hasan, Unconventional chiral charge order in kagome superconductor KV_3Sb_5 , *Nature Materials* 10.1038/s41563-021-01034-y (2021).
 - [17] C. M. III, D. Das, J.-X. Yin, H. Liu, R. Gupta, C. Wang, Y.-X. Jiang, M. Medarde, X. Wu, H. Lei, J. Chang, P. Dai, Q. Si, H. Miao, R. Thomale, T. Neupert, Y. Shi, R. Khasanov, M. Hasan, H. Luetkens, and Z. Guguchia, Time-reversal symmetry-breaking charge order in a correlated kagome superconductor (2021), arXiv:2106.13443 [cond-mat.str-el].
 - [18] L. Yu, C. Wang, Y. Zhang, M. Sander, S. Ni, Z. Lu, S. Ma, Z. Wang, Z. Zhao, H. Chen, K. Jiang, Y. Zhang, H. Yang, F. Zhou, X. Dong, S. L. Johnson, M. J. Graf, J. Hu, H.-J. Gao, and Z. Zhao, Evidence of a hidden flux phase in the topological kagome metal csv_3sb_5 (2021), arXiv:2107.10714 [cond-mat.str-el].
 - [19] N. Shumiya, M. S. Hossain, J.-X. Yin, Y.-X. Jiang, B. R. Ortiz, H. Liu, Y. Shi, Q. Yin, H. Lei, S. S. Zhang, G. Chang, Q. Zhang, T. A. Cochran, D. Multer, M. Litskevich, Z.-J. Cheng, X. P. Yang, Z. Guguchia, S. D. Wilson, and M. Z. Hasan, Intrinsic nature of chiral charge order in the kagome superconductor Rbv_3sb_5 , *Phys. Rev. B* **104**, 035131 (2021).

- [20] H. Zhao, H. Li, B. R. Ortiz, S. M. L. Teicher, T. Park, M. Ye, Z. Wang, L. Balents, S. D. Wilson, and I. Zeljkovic, Cascade of correlated electron states in a kagome superconductor csv_3sb_5 (2021), arXiv:2103.03118 [cond-mat.supr-con].
- [21] H. Chen, H. Yang, B. Hu, Z. Zhao, J. Yuan, Y. Xing, G. Qian, Z. Huang, G. Li, Y. Ye, Q. Yin, C. Gong, Z. Tu, H. Lei, S. Ma, H. Zhang, S. Ni, H. Tan, C. Shen, X. Dong, B. Yan, Z. Wang, and H.-J. Gao, Roton pair density wave and unconventional strong-coupling superconductivity in a topological kagome metal (2021), arXiv:2103.09188 [cond-mat.supr-con].
- [22] Z. Wang, Y.-X. Jiang, J.-X. Yin, Y. Li, G.-Y. Wang, H.-L. Huang, S. Shao, J. Liu, P. Zhu, N. Shumiya, M. S. Hossain, H. Liu, Y. Shi, J. Duan, X. Li, G. Chang, P. Dai, Z. Ye, G. Xu, Y. Wang, H. Zheng, J. Jia, M. Z. Hasan, and Y. Yao, Electronic nature of chiral charge order in kagome superconductor csv_3sb_5 (2021), arXiv:2105.04542 [cond-mat.supr-con].
- [23] D. Wulferding, S. Lee, Y. Choi, Q. Yin, Z. Tu, C. Gong, H. Lei, and K.-Y. Choi, Fermi surface instabilities in electronic raman scattering of the metallic kagome lattice csv_3sb_5 (2021), arXiv:2108.11690 [cond-mat.supr-con].
- [24] Y. Xiang, Q. Li, Y. Li, W. Xie, H. Yang, Z. Wang, Y. Yao, and H.-H. Wen, Twofold symmetry of c -axis resistivity in topological kagome superconductor csv_3sb_5 with in-plane rotating magnetic field (2021), arXiv:2104.06909 [cond-mat.supr-con].
- [25] J. Luo, Z. Zhao, Y. Z. Zhou, J. Yang, A. F. Fang, H. T. Yang, H.J.Gao, R.Zhou, and G. qing Zheng, Star-of-david pattern charge density wave with additional modulation in the kagome superconductor csv_3sb_5 revealed by ^{51}V -nmr and $^{121/123}\text{Sb}$ -nqr (2021), arXiv:2108.10263 [cond-mat.supr-con].
- [26] G. Grüner, *Density Waves in Solids* (CRC Press, Taylor & Francis Group, Boca Raton, 2018) pp. 1–288.
- [27] K. Rossnagel, On the origin of charge-density waves in select layered transition-metal dichalcogenides, *Journal of Physics: Condensed Matter* **23**, 213001 (2011).
- [28] M. Spera, A. Scarfato, A. Pásztor, E. Giannini, D. R. Bowler, and C. Renner, Insight into the charge density wave gap from contrast inversion in topographic stm images, *Phys. Rev. Lett.* **125**, 267603 (2020).
- [29] A. H. Said, H. Sinn, T. S. Toellner, E. E. Alp, T. Gog, B. M. Leu, S. Bean, and A. Alatas, High-energy-resolution inelastic X-ray scattering spectrometer at beamline 30-ID of the Advanced Photon Source, *Journal of Synchrotron Radiation* **27**, 827 (2020).
- [30] T. S. Toellner, A. Alatas, and A. H. Said, Six-reflection meV-monochromator for synchrotron radiation, *Journal of Synchrotron Radiation* **18**, 605 (2011).
- [31] A. Q. Baron, Introduction to high-resolution inelastic x-ray scattering, arXiv (2015), arXiv:1504.01098v2.
- [32] See Supplemental Materials at <http://...>
- [33] H. Miao, J. Lorenzana, G. Seibold, Y. Y. Peng, A. Amorese, F. Yakhov-Harris, K. Kummer, N. B. Brookes, R. M. Konik, V. Thampy, G. D. Gu, G. Ghiringhelli, L. Braicovich, and M. P. M. Dean, High-temperature charge density wave correlations in $\text{La}_{1.875}\text{Ba}_{0.125}\text{CuO}_4$ without spin-charge locking, *Proceedings of the National Academy of Sciences* **114**, 12430 (2017), <https://www.pnas.org/content/114/47/12430.full.pdf>.
- [34] H. Miao, G. Fabbris, R. J. Koch, D. G. Mazzone, C. S. Nelson, R. Acevedo-Esteves, G. D. Gu, Y. Li, T. Yilmaz, K. Kaznatcheev, E. Vescovo, M. Oda, T. Kurosawa, N. Momono, T. Assefa, I. K. Robinson, E. S. Bozin, J. M. Tranquada, P. D. Johnson, and M. P. M. Dean, Charge density waves in cuprate superconductors beyond the critical doping, *npj Quantum Materials* **6**, 31 (2021).
- [35] Z. Wang, Y.-X. Jiang, J.-X. Yin, Y. Li, G.-Y. Wang, H.-L. Huang, S. Shao, J. Liu, P. Zhu, N. Shumiya, M. S. Hossain, H. Liu, Y. Shi, J. Duan, X. Li, G. Chang, P. Dai, Z. Ye, G. Xu, Y. Wang, H. Zheng, J. Jia, M. Z. Hasan, and Y. Yao, Electronic nature of chiral charge order in kagome superconductor csv_3sb_5 (2021), arXiv:2105.04542 [cond-mat.str-el].
- [36] Q. Yin, Z. Tu, C. Gong, Y. Fu, S. Yan, and H. Lei, Superconductivity and normal-state properties of kagome metal rbv_3sb_5 single crystals, *Chinese Physics Letters* **38**, 037403 (2021).